Tunable quantum switch realized with a single Λ-level atom coupled to the microtoroidal cavity

Davit Aghamalyan,[1] Jia-Bin You,[2] Hong-Son Chu,[2] Ching Eng Png,[2] Leonid Krivitsky,[3] and Leong Chuan Kwek[4,1,5]
[1]*Centre for Quantum Technologies, National University of Singapore, 3 Science Drive 2, Singapore 117543*
[2]*Institute of High Performance Computing, A*STAR (Agency for Science, Technology and Research), 1 Fusionopolis Way, #16-16 Connexis, Singapore 138632*
[3]*Institute of Materials Research and Engineering, A*STAR (Agency for Science, Technology and Research), 2 Fusionopolis Way, #08-03 Innovis, Singapore 138634*
[4]*MajuLab, CNRS-UNS-NUS-NTU International Joint Research Unit, UMI 3654, Singapore*
[5]*National Institute of Education and Institute of Advanced Studies, Nanyang Technological University, 1 Nanyang Walk, Singapore 637616*

(Received 7 July 2019; published 22 November 2019)

We propose a realization of the quantum switch for coherent light fields for the fiber-coupled microdisk cavities. We demonstrate by combining numerical and analytical methods that both in strong coupling and bad cavity limits it is possible to change a system's behavior from being fully transparent to being fully reflective by varying the amplitude of the external control field. We remark that tuning the amplitude of the control field instead of cavity-atom coupling strength, which was suggested by S. Parkins *et al.*, [Phys. Rev. A **90**, 053822 (2014)] for two-level atoms and works only in the strong coupling limit, brings more control and tunability over the transmitted and reflected intensities. We also demonstrate the possibility of controlling the statistics of the input coherent field with the control field which opens the venue for obtaining quantum states of light.

DOI: 10.1103/PhysRevA.100.053851

I. INTRODUCTION

Quantum networks [1] provide a prominent template for the design and realization of scalable quantum information processing systems. Quantum network consists of nodes, which are formed with a physical system such as atoms. Nodes are then linked together through the quantum channel, and this is usually done with the help of photons referred to in this context as "flying qubits." The interaction between light and matter establishes the transfer and the manipulation of information between the "flying qubits" and the nodes. Quantum networks may eventually play an important role in the future implementation of quantum computation, communication, and metrology [2–6].

Trapped atoms in Fabry-Perot cavities have been one of the most fruitful systems for testing fundamentals of quantum optics in cavity QED setup [7–10]. Single atoms in Fabry-Perot cavities have been demonstrated to be good candidates for a quantum network [8,11–14]; however, it turns out that these cavities fail to realize large-scale networking. To overcome this issue, several types of microchip-based systems(microdisk, micropillar, microbottle, and photonic crystal cavities) [15] have been engineered and successfully utilized for implementing cavity-QED type of experiments [16–22] by coupling them with trapped cold atoms, quantum dots. Numerical and theoretical methods have also been developed to understand the optical properties of these systems [23–26].

Microtoroidal and microdisk cavities hold a promise to realize scalable quantum networks and are fascinating platforms for realizing quantum optical experiments since the electrical field, with its small mode volume, reaches high values inside the cavity resulting in a large light-matter coupling. Experimentally, the strong coupling regime has been successfully reported for such systems [16–19]. Due to their small losses, these systems have high quality factors (Q) and, in one experiment, Q as large as 4×10^8 have been realized [20]. Moreover, by coupling tapered fiber with ring resonator the efficiency of coupling light in and out of the microtoroidal resonator can achieve up to 0.997 as demonstrated experimentally in Ref. [16].

Photonic quantum devices [27] are necessary components for implementing functional quantum network, and they play an important role in storing the quantum states of light, as well in controlling the propagation of light. Switching the direction of the propagating is one of the most important operations that need to be performed in the quantum network. To achieve this task a quantum switch [28–34] is needed and is implemented by changing an external parameter, which results in "on" or "off" state of the switch, much like a gate valve in a water pipe. If this device is implemented solely through optical means, then this kind of switch is called "all optical switch" [29–31,35]. Quantum switch acts as "gate valves" for quantum states of light [9,36–39]. Both theoretical proposals [38,40,41] along with actual experimental implementations [28,29,31] for realizing single-photon transistor have been put forward.

In this paper, we focus on the realization of a quantum switch for an incoming coherent field. An interesting result that quantum communication between two atomic ensembles can be achieved by means of only coherent laser fields has been theoretically proposed [42] and later an entanglement between two atomic ensembles has been experimentally demonstrated in Ref. [43]. These findings demonstrate that quantum network can be formed with only coherent laser fields which overcomes the difficulty of creating quantum states of light(it is an outstanding challenge to have single-photon source) for realizing quantum communication.

In Ref. [44], Parkins and Aoki suggested an interesting scheme for the coherent light quantum switch by utilizing clockwise and anticlockwise cavity mods of the whispering gallery modes (WGM) of the ring resonator [23,45]. They showed that, under certain parameter regime (strong cavity-fiber coupling along with strong cavity-atom coupling), it is possible to achieve a coherent light switch by tuning cavity-atom interaction strength g going from weak coupling to strong coupling regimes.

Here, we highlight, that controlling the interaction strength g in the actual experiments could be very challenging because one needs to modify the distance between the atoms and ring cavity to modify the evanescent coupling. To overcome this issue an auxiliary level was introduced and with radio-frequency pulse atom could be shifted into this level which effectively decouples atom from the cavity and achieves "off" state of the switch. However, this approach allows only for very high value of g or $g = 0$ and omits intermediate values of g, which results only in partial control over transmitted and reflected intensities and their respective photon statistics.

To cure this issue it is desirable to have an easily tunable external parameter. Here we propose to replace the two-level atom with a three-level atom in a Λ-level configuration and the "gate valve" is implemented by tuning the amplitude of the control field. In several theoretical articles [41,46,47] the system of a three-level atom coupled to the microtoroidal cavity has been theoretically investigated; however, in all these papers the typical EIT condition of zero two-photon detuning has been assumed. Contrarily, for our protocol it is crucial to have nonzero two-photon detuning; otherwise, because of the coherent population trapping mechanism system behaves as transparent for any value of control field, because of the optical pumping into the dark state [9,36].

In this manuscript, we argue that a quantum switch, controlled by varying the amplitude of the external field, gives more control and tunability over transmitted and reflected intensities(for example 50/50 beam splitter cane be achieved with our scheme). Moreover, our protocol for a switch works even in the bad-cavity limit, which overcomes experimental effort to bring the system in the strong coupling regime. However, it is important to point out that contrary to the strong coupling regime where reflected light does not change its statistics, in the bad cavity limit it becomes quantum after being reflected.

The manuscript is outlined as follows. In Sec. II, we provide a theoretical description of the system and set the stage for the numerical simulations of the master equation that governs the system dynamics. In Sec. III, we demonstrate, both numerically and analytically, that our system functions as a quantum switch for an incoming coherent field (even within the bad cavity limit). In Sec. IV, we study the statistics of the transmitted and reflected fields, in strong coupling and bad cavity limits. In Sec. V we briefly outline the scheme for generating light-matter entanglement, which is consequently used to produce a cat state. Section VI is devoted to our conclusions. In the Appendix analytical results for the bad-cavity limit are derived using adiabatic elimination of the cavity modes.

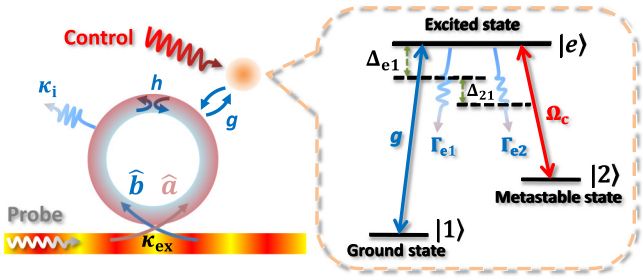

FIG. 1. Scheme of a three-level atom coupled to a ring cavity and a tapered-fiber. Input fields $a_{\text{in,ex}}, b_{\text{in,ex}}$ propagate through the fiber which is coupled with a rate κ_{ex} with a microtoroid cavity which has a resonant frequency of ω_r. Coherent probe field of frequency ω_p drives the mode a with strength Ω_p. Two counterpropagating WGM modes a and b are assumed to be coupled with a strength h due to the scattering from imperfections. Both modes can leak out of the cavity with a rate κ_{i}, and the outgoing fields resulting from the fiber are given by the $a_{\text{out,ex}}, b_{\text{out,ex}}$. Degenerate cavity modes a and b are coupled with the three-level atom and drive the transition $1 - e$. Control field with amplitude Ω_c and the frequency ω_c drives the transition $2 - e$. Atomic populations of the excited state e can decay through two decay channels either to the state 1 or to the state 2.

II. THE SYSTEM AND THE MASTER EQUATION FORMALISM

A schematic representation of the system along with main parameter definitions is given in Fig. 1. It is important to point out that once the anticlockwise WGM mode a is created, there are two different mechanisms that can give rise to the clockwise mode b. The first mechanism is the evanescent coupling with a strength g with the two-level atom since atom can re-emit the photon in both directions: clockwise and anticlockwise. The second mechanism is a result of the inhomogeneity of the dielectric media and is described by the parameter h (for more details, see Ref [25]). In this paper we will focus mainly on the case with $h = 0$.

In a rotating frame $U(t) = e^{i\omega_p t(a^\dagger a + b^\dagger b - \sigma_{11}) - i\omega_c t\sigma_{22}}$, the Hamiltonian of the system takes the form

$$\begin{aligned} H =& \Delta_r(a^\dagger a + b^\dagger b) + h(a^\dagger b + b^\dagger a) + \Delta_{e1}\sigma_{ee} + \Delta_{21}\sigma_{22} \\ &+ (g^* a^\dagger \sigma_{1e} + g a\sigma_{e1}) + (g b^\dagger \sigma_{1e} + g^* b\sigma_{e1}) \\ &+ \Omega_p(a + a^\dagger) + \Omega_c(\sigma_{2e} + \sigma_{e2}), \end{aligned} \tag{1}$$

where $\Delta_r = \omega_r - \omega_p$, $\Delta_{e1} = \omega_{e1} - \omega_p$ and $\Delta_{21} = \omega_{21} + \omega_c - \omega_p$. After introducing the dissipative channels the system within the the Born- MArkov approximation is described by the Lindblad master equation (here we assume zero temperature thermal reservoir):

$$\begin{aligned} \dot{\rho} =& -i[H, \rho] + \kappa\mathcal{D}[a]\rho + \kappa\mathcal{D}[b]\rho \\ &+ \frac{\Gamma_{e1}}{2}\mathcal{D}[\sigma_{1e}]\rho + \frac{\Gamma_{e2}}{2}\mathcal{D}[\sigma_{2e}]\rho, \end{aligned} \tag{2}$$

where $\mathcal{D}[\hat{o}]\rho = 2\hat{o}\rho\hat{o}^\dagger - \hat{o}^\dagger\hat{o}\rho - \rho\hat{o}^\dagger\hat{o}$ is the Lindblad superoperator and $\kappa = \kappa_{\text{ex}} + \kappa_{\text{i}}$, Γ_{e1}, Γ_{e2} are the decay rates of a cavity and an atom respectively. It is important to highlight that throughout the manuscript the condition of weak

coupling($g/\omega_{c,e} < 0.1$) is satisfied, and rotating approximation holds and Linblad operators do not require modification.

A. Input-output formulation of the system

The input and output fields which are schematically shown in Fig. 1 and are related through the input-output relations (see Chapter 7 of Ref. [48]) in the Heisenberg picture and are given by the following expressions:

$$\begin{aligned} a_{\mathrm{out,ex}}(\tau) &= -a_{\mathrm{in,ex}}(\tau) + \sqrt{2\kappa_{\mathrm{ex}}}a(\tau), \\ b_{\mathrm{out,ex}}(\tau) &= -b_{\mathrm{in,ex}}(\tau) + \sqrt{2\kappa_{\mathrm{ex}}}b(\tau), \end{aligned} \tag{3}$$

where input and output fields have delta function commutation relations in time. The field Ω_p in the Hamiltonian corresponds to the coherent field incoming from the left and input field incoming from the right is assumed to be in the vacuum state, which is given by the average values of the input operators:

$$\langle a_{\mathrm{in}}\rangle = -\frac{i\Omega_p}{\sqrt{2\kappa_{\mathrm{ex}}}}, \quad \langle b_{\mathrm{in}}\rangle = 0. \tag{4}$$

The transmission and the reflection coefficients, normalized to the input photon flux number, are given by

$$T = \frac{\langle a^{\dagger}_{\mathrm{out,ex}} a_{\mathrm{out,ex}}\rangle}{|\Omega_p|^2/2\kappa_{\mathrm{ex}}}, \quad R = \frac{\langle b^{\dagger}_{\mathrm{out,ex}} b_{\mathrm{out,ex}}\rangle}{|\Omega_p|^2/2\kappa_{\mathrm{ex}}}. \tag{5}$$

B. Normal mode decomposition

To achieve a better understanding of the system, it is instructive to rewrite the Hamiltonian in terms of the normal modes of cavity A and B, defined as $A = \frac{a+b}{\sqrt{2}}$, $B = \frac{a-b}{\sqrt{2}}$. After expressing a and b through the normal modes, the Hamiltonian of the system reads as

$$\begin{aligned} H_{\mathrm{N.M.}} =& \Delta_{e1}\sigma_{ee} + \Delta_{21}\sigma_{22} + (\Delta_r + h)A^{\dagger}A + (\Delta_r - h)B^{\dagger}B \\ &+ g_A(A^{\dagger}\sigma_{1e} + \sigma_{1e}A) + g_B(B^{\dagger}\sigma_{1e} + \sigma_{1e}B) \\ &+ \Omega_c(\sigma_{2e} + \sigma_{e2}) + \frac{\Omega_p}{\sqrt{2}}(B + B^{\dagger}) + \frac{\Omega_p}{\sqrt{2}}(A + A^{\dagger}), \end{aligned} \tag{6}$$

where g_A and g_B, are given by

$$g_A = \sqrt{2}g_0 f(r)\cos(kx),\ g_B = \sqrt{2}g_0 f(r)\sin(kx). \tag{7}$$

Here g_0 is the amplitude of the stationary electromagnetic field in the ring oscillator and $f(r)$ is the radial distribution function of the electromagnetic field. Equation (7) shows that by properly choosing the location of the atom along the ring cavity, it is possible to decouple one of the cavity modes. In the rest of the manuscript it is assumed that $\sin(kx) = 0$, so that the mode B is decoupled from the atom. Ring optical resonators such as microtoroids do not support circularly polarized modes [1]. Counterpropagating transverse electric (TE) modes create a pair of orthogonal standing-wave normal modes (A and B), and the phase of one of these modes can always be chosen so that it has a node at the position of the atom. It is easy to notice from the expression for $H_{\mathrm{N.M.}}$ that there are no terms in the Hamiltonian that couple mode B with the atom or with other normal mode A (that terms are given by the two last lines in Eq. (6) and we denote that part of Hamiltonian as H_B). This in turn implies that systems $\Sigma + A$ (here Σ represents the subspace of a two-level atom) and B are noninteracting and the full system Hamiltonian and the density matrix can be expressed as

$$H_{\mathrm{N.M.}} = H_{\Sigma+A} + H_B, \tag{8}$$

$$\rho = \rho_{\Sigma+A} \otimes \rho_B. \tag{9}$$

Next, we proceed to write the master equation of the system in the normal mode basis

$$\begin{aligned} \dot{\rho} =& -i[H_{\mathrm{N.M.}}, \rho] + \kappa\mathcal{D}[A]\rho + \kappa\mathcal{D}[B]\rho \\ &+ \frac{\Gamma_{e1}}{2}\mathcal{D}[\sigma_{1e}]\rho + \frac{\Gamma_{e2}}{2}\mathcal{D}[\sigma_{2e}]\rho. \end{aligned} \tag{10}$$

After substituting Eq. (9) into Eq. (10) and tracing out separately the subsystems $\Sigma + A$ and B, equations for the respective subsystems take the following form:

$$\begin{aligned} \dot{\rho}_{\Sigma+A} =& -i[H_{\Sigma+A}, \rho_{\Sigma+A}] + \kappa\mathcal{D}[A]\rho_{\Sigma+A} \\ &+ \frac{\Gamma_{e1}}{2}\mathcal{D}[\sigma_{1e}]\rho_{\Sigma+A} + \frac{\Gamma_{e2}}{2}\mathcal{D}[\sigma_{2e}]\rho_{\Sigma+A}, \end{aligned} \tag{11}$$

$$\dot{\rho}_B = -i[H_B, \rho_B] + \kappa\mathcal{D}[B]\rho_B. \tag{12}$$

It is important to notice that Eqs. (11) and (12) present a significant numerical advantage compared to Eq. (2), since in the first case full system density matrix is obtained (as a tensor product) by solving two separate equations for density matrices of dimension $O(n)$, contrary to the second case where one equation for the full system density matrix of the dimension $O(n^2)$ has to be solved; here n shows truncation number of the Fock state for the cavity modes.

III. QUANTUM SWITCH

The main result of this manuscript is shown in Fig. 2 and is obtained by numerical simulations of master Eqs. (11) and (12) which takes into account all dissipative channels. Here we use the superspace method which is outlined in a great detail in Ref. [49]. Moreover, analytical results for the bad cavity limit ($g < \kappa_{\mathrm{ex}}$), which are outlined in detail in the Appendix, are also plotted in Fig. 2 for comparison with numerics. In Fig. 2 transmission and reflection are plotted as a function of the amplitude of the control field, for the set of parameters given in the caption. For the system parameters we use the realistic experimental values taken from Ref. [16], where SiO_2 microtoroidal resonator was coupled with a cloud of cold cesium atoms. For cesium atoms considering the transition $6S_1/2, F = 4 \rightarrow 6P_{3/2,}, F' = 5'$, and taking into account selection rules imposed by linearly polarized light of the cavity field ($\Delta m_F = 0$) for the Zeeman states $\{m_F\}$, we can choose, for example, $6S_{1/2}, F = 4, m_F = -4 \rightarrow 6P_{3/2}, F' = 5', m_{F'} = -4$. For some range of Ω_c, $T \approx 0$, and $R \approx 1$ (we remark that $T + R < 1$ due to the losses in the system), which means that the system works as a quantum switch. Transmission and reflection curves have two crossing points and for both points $T = R \approx 0.5$ which means the systems works as a 50/50 beam splitter for an incoming coherent field. To gain better understanding about the behavior of transmitted and reflected intensities, in the right column of Fig. 2 we

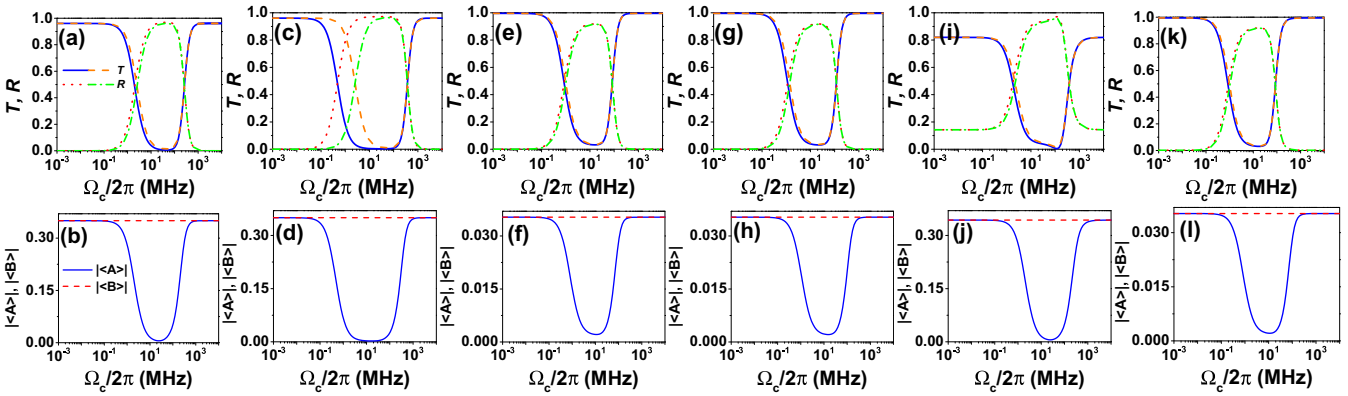

FIG. 2. Normalized power transmission T, reflection R, and the populations of normal modes A and B as a function of control field strength Ω_c. The blue and red solid lines are transmission and reflection functions resulting from the master equation simulations, respectively. The orange and green dashed lines are transmission and reflection functions resulting from adiabatic elimination, respectively. The parameters for strong coupling cases are $\{\Delta_r, \Delta_{e1}, h, g, \Omega_p, \kappa_{\rm ex}, \kappa_{\rm i}, \Gamma_{e1}, \Gamma_{e2}\}/2\pi = \{0, 0, 0, 100, 10, 20, 0.2, 5.2, 5.2\}$ MHz and (a), (b) $\Delta_{21}/2\pi = 70$ MHz; (c), (d) $\Delta_{21}/2\pi = 140$ MHz. The parameters for bad cavity cases are $\{\Delta_r, \Delta_{e1}, h, g, \Omega_p, \kappa_{\rm ex}, \kappa_{\rm i}, \Gamma_{e1}, \Gamma_{e2}\}/2\pi = \{0, 0, 0, 100, 10, 200, 0.2, 5.2, 5.2\}$ MHz and (e), (f) $\Delta_{21}/2\pi = 70$ MHz; (g), (h) $\Delta_{21}/2\pi = 140$ MHz. For the cases of nonzero h, the parameters are $\{\Delta_r, \Delta_{e1}, \Delta_{21}, h, g, \Omega_p, \kappa_{\rm i}, \Gamma_{e1}, \Gamma_{e2}\}/2\pi = \{0, 0, 70, 4, 100, 10, 0.2, 5.2, 5.2\}$ MHz and (i), (j) $\kappa_{\rm ex}/2\pi = 20$ MHz for strong coupling case; (k), (l) $\kappa_{\rm ex}/2\pi = 200$ MHz for bad-cavity case.

plot the amplitudes of the modes A and B as a function of Ω_c. The mode B is decoupled from an atom so its population stays constant; however, mode A is strongly coupled to the atom, which in turn is coupled to the external control field, and for some range of the control field amplitude the mode A is going out of resonance, and this range coincides with the range where transmission goes to zero which is apparent by comparing the first and the second columns in Fig. 2. This behavior can be easily explained by expressing the output field $a_{\rm out,ex} = -a_{\rm in,ex} + \sqrt{\kappa}(A + B)$, through the normal modes, and taking into account that in the switch region $\langle A\rangle \approx 0$. Since the normal mode B is decoupled from the atom, its average value can be obtained by solving steady-state equations for the empty cavity($g = 0$). As it is shown in the Appendix, it follows from the Eq. (A2) that in the case $\Delta_r = 0$ and $h = 0$, $\sqrt{\kappa}\langle B\rangle = \langle a_{\rm in,ex}\rangle$. Under mean-field approximation, $T \approx \langle a^\dagger_{\rm out,ex}\rangle\langle a_{\rm out,ex}\rangle \approx 0$, because of the destructive interference between the input field and the mode B. Here, to estimate the intensity we applied a mean-field approximation which is not assumed later in the manuscript. The condition $\langle A\rangle \approx 0$ implies that mode a and b have the same amplitude with opposite sign, this means that atom in a way is acting like a pump which is redistributing photon fluxes between these two modes and ones this two modes get equally populated system is acting as a "mirror." From Fig. 2 it is seen that for small value and large values of control fields atom is "effectively" getting decoupled from the cavity. For small values of Ω_c, this happens simply because atom is getting optically pumped to the level 2, since $|\omega_{1e} - \omega_{2e}| \gg \gamma_{1e}, \gamma_{2e}$. For the large values of Ω_c, the atom-field dressed energy level gets detuned on the large amount $\approx\Omega_c \gg \gamma_{1e}, \gamma_{2e}$ and cavity mode gets out of resonance with the dressed light atom energy state. This statements are substantiated by analytical results for the bad cavity limit which are presented in the Appendix. As it is demonstrated there for both limits of very small and very large Ω_c, $\rho_{1e} \approx 0$, which means that absorption is vanishing and light is propagating through the cavity without "feeling" the atom. Figures 2(i), 2(j) and 2(k), 2(l) illustrate the effect of nonzero h. In general, a nonzero h induces coupling between the clockwise and anticlockwise cavity modes, and weakens the switch functionality in the strong coupling regime yet it almost does not modify it in bad-cavity limit (here $h < \kappa$). To gain intuition on this, it is instructive to consider at first the case when of empty cavity. When $g = 0$, the backscattering causes mode splitting (when backscattering rate h exceeds all other losses in the system κ) and distinct pair of resonances emerges at the frequencies $\omega_c \pm h$; however, in the bad cavity limit this effect is getting washed out. This results in asymmetric transmission/reflection profiles in the strong coupling limit which agrees well with findings for the two-level atom coupled to the microtoroidal cavity studied in depth in Ref. [25]. To avoid detrimental effects introduced by h in the strong coupling limit it is enough to be in the regime $h \ll \kappa$.

An interesting feature of our system, that switch functionality regime can be made wider by changing the two-photon detuning, is apparent, for example, by comparing Fig. 2(a), where $\Delta_{12} = 70$ MHz, with Fig. 2(c) (strong-coupling limit), where $\Delta_{12} = 140$ MHz. Moreover, from Figs. 2(e) and 2(g) we see that in the bad-cavity limit, analytical curves, given by the dashed lines, agree well with numerical simulations of master equations, given by blue and red curves. This agreement quite remarkably holds partially even in the strong coupling limit, which is apparent from Fig. 2(a) (however, analytical results for the two-photon correlation functions agree with numerics only in the bad-cavity limit). As we can see from the second column of Fig. 2, average value of the mode A is one order of magnitude bigger in the bad-cavity limit, which results in having better switch in the strong coupling limit where transmission turns out to be smaller on one order of magnitude compared to the bad-cavity case. We comment, that the fact that mode $\langle A\rangle$ is bigger in the bad-cavity limit manifests itself in having different statistics for the reflected field in this limit compared to the strong coupling-limit, which we discuss in more detail in Sec. IV.

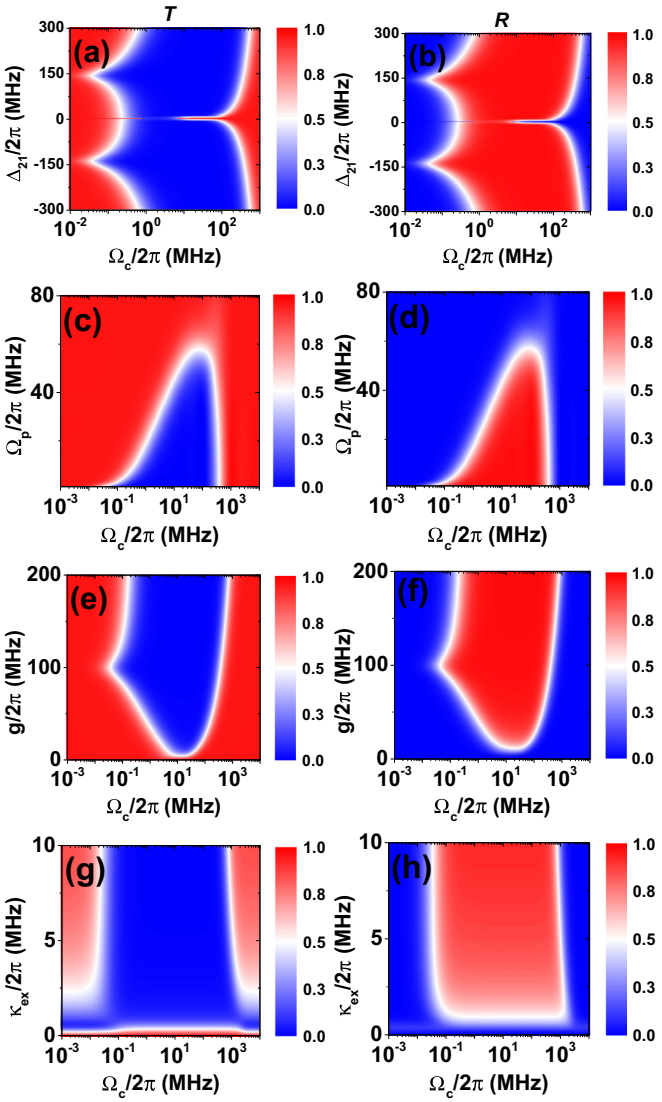

FIG. 3. Contour plots for transmission and reflection profiles in strong coupling regime. The parameters are the same as in Fig. 2(c) except $\Omega_p = 1$.

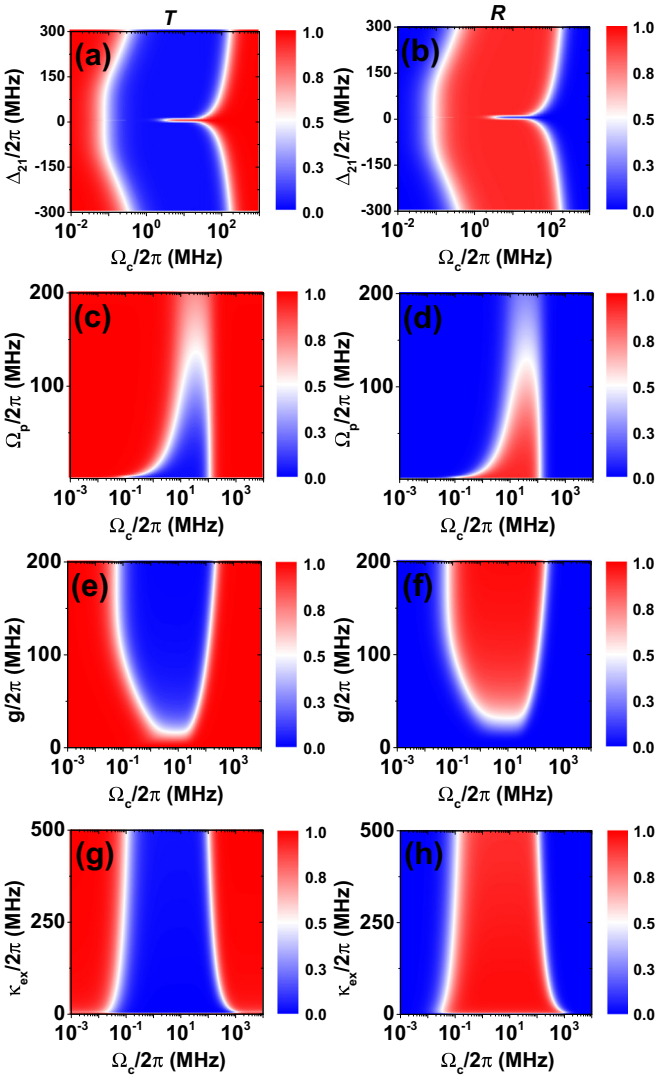

FIG. 4. Contour plots for transmission and reflection profiles in bad-cavity regime. The parameters are the same as in Fig. 2(g) except $\Omega_p = 1$.

Bigger is the range of Ω_c over which the system works as a quantum transistor; better is the quantum switch. To understand why is this the case it is constructive to consider the opposite limit when this range is extremely narrow, then experimental imperfections and noise can easily push the system out of the regime of functionality. Bearing this in mind, we make a series of contour plots for exploring the parameter regimes where the "range of functionality" is broad. In these contour plots, one axis represents the external control field and other axis denotes the physical parameter of interest. Figure 3 shows the series of contour plots where the left and right columns show transmission and reflection intensities. Range of functionality is given by the length of horizontal line (for a given value of parameter along the y axis) which has a dark/blue color corresponding to $T \approx 0$. In Figs. 3(a) and 3(b) we plot T and R in the Δ_{21}-Ω_p plane, in the strong-coupling limit. For the small value of Ω_c we see double-peak structure which is a signature of vacuum Rabi splitting, because for the small value of control field excited state is splitting in the Jaynes-Cummings doublet, and peaks are located at $\approx\sqrt{2}g$. The factor $\sqrt{2}$ is a result of having standing waves in the microtoroidal cavity. From this figures, we conclude, that for a switch with a wide rang of functionality the optimal value of two photon detuning should be chosen equal $\Delta_{21} \approx \sqrt{2}g$. From Figs. 4(a) and 4(b) we see that, in principle, many values of two-photon detuning realize a good switch because in this case there is no vacuum Rabi splitting, and consequently no Rabi oscillations occur, as photons leave the cavity before being reabsorbed by the atom. However, for being consistent we also choose $\Delta_{21} \approx \sqrt{2}g$.

The transmission/reflection in Ω_p-Ω_c plane is shown in Figs. 3(c) and 3(d), in the strong-coupling limit. With increasing amplitude of the input drive field, the range over which switch functions (i.e., the dark/red region) narrows until it completely disappears. This behavior occurs as a result of an atom being saturated on the $1 - e$ transition. So the weaker is the amplitude of the input field, the better switch can function.

We remark, that onset of saturation occurs for smaller value of Ω_p, in the bad cavity limit [see Figs. 4(c) and 4(d)], because in this limit atom gets saturated with relatively small number of photons. Moreover, in the bad-cavity limit the range of functionality for a given value of Ω_p, is narrower compared to the strong-coupling limit. The transmission/reflection in g-Ω_p plane is shown in Figs. 3(e) and 3(f). For very small values of g, photons will pass through the cavity without interacting with the atom which means $T \approx 1$ and system does not perform as a switch. We remark that since here $h = 0$, the only way for producing anticlockwise photons is through interaction with the atom. If g is too small, then the atom is decoupled from the cavity, and if g is too big, then the cavity field will be off resonant with the atoms due to the large energy level shift, so consequently there is an optimal value for g which provides widest regime of functionality which is apparent from Fig. 3(e). Here, we see that for a fixed two-photon detuning Δ_{21}, there is an optimal value of g given by $g \approx \Delta_{21}/\sqrt{2}$ in agreement with existence vacuum Rabi splitting as was discussed above. Same kind of behavior is observed in the bad-cavity limit [see Figs. 4(e) and 4(f)], except in this regime there is no optimal value of g for a given two-photon detuning, because of the absence of vacuum Rabi splitting.

Transmitted and reflected intensities in $\kappa_{\rm ex}$-Ω_p plane are shown in Figs. 3(e) and 3(f). Here we see that system performs as a switch both in strong-coupling ($\kappa_{\rm ex} < 100$) and bad-cavity ($\kappa_{\rm ex} > 100$) limits, showing wider range of functionality in the strong coupling limit in agreement with our findings for the saturation behavior. In Figs. 3(g) and 3(h) we show a zoom of Figs. 4(g) and 4(h), as it reveals an interesting feature. System is performing as a switch only in the fiber-overcoupling regime which is given by the condition $\kappa_{\rm ex} \gg \kappa_i$, this condition ensures high efficiency of the input-output transfer of the light, which is obviously a necessary condition for a strong light-matter interaction.

IV. PHOTON STATISTICS

In this section, we study the photon statistics for the transmitted and reflected light fields, both in strong coupling and bad-cavity limits. Here we mainly focus on regions where quantum switch is functioning, which means $T \approx 0$. In this region, most of the photon flux is reflected and our main focus here is to study the statistics of the reflected light; however, since a small number of photons is passing in the forward direction two-photon correlation function still can be observed through photodetection. Two-photon correlation functions for transmitted and reflected fields are defined through the output fields as follows:

$$g_{\rm T}^{(2)}(0) = \frac{\langle a_{\rm out,ex}^{\dagger} a_{\rm out,ex}^{\dagger} a_{\rm out,ex} a_{\rm out,ex}\rangle_{\rm ss}}{(\langle a_{\rm out,ex}^{\dagger} a_{\rm out,ex}\rangle_{\rm ss})^2},$$

$$g_{\rm R}^{(2)}(0) = \frac{\langle b_{\rm out,ex}^{\dagger} b_{\rm out,ex}^{\dagger} b_{\rm out,ex} b_{\rm out,ex}\rangle_{\rm ss}}{(\langle b_{\rm out,ex}^{\dagger} b_{\rm out,ex}\rangle_{\rm ss})^2}. \quad (13)$$

If $g^{(2)}(0) < 1$ (e.g., for the field in the Fock state $|n\rangle$, it can be easily shown that $g^{(2)}(0) = 1 - 1/n$), then the field has sub-Poissonian statistics. If $g^{(2)}(0) = 1$ (e.g., any coherent field $|\alpha\rangle$), then the field has a Poissonian statistics. Finally,

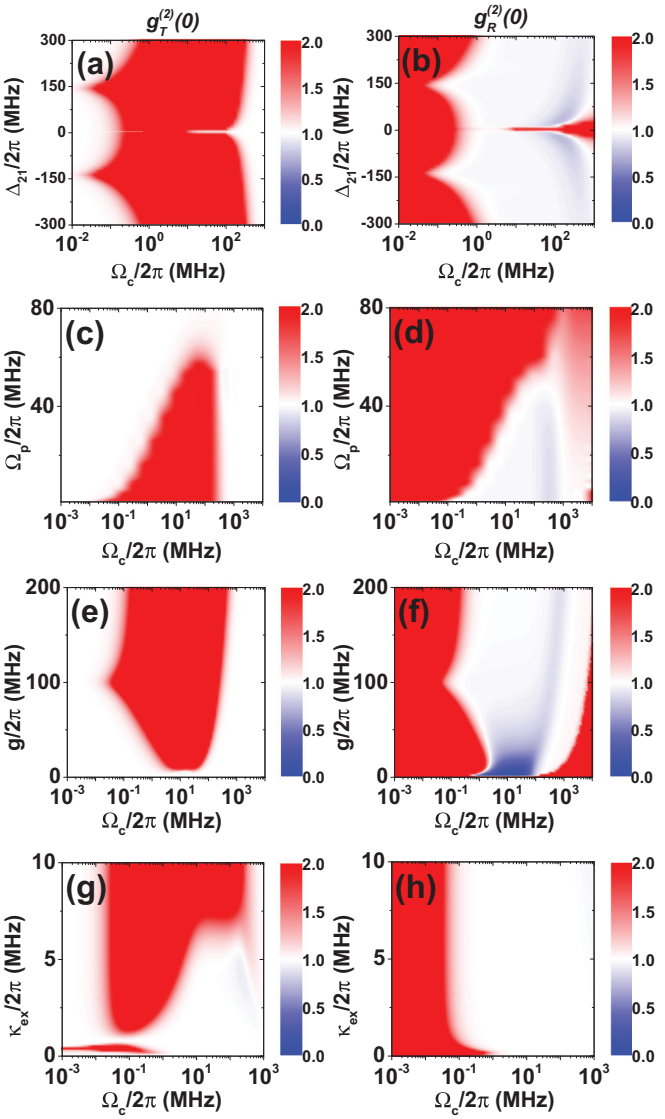

FIG. 5. Contour plots for the photon statistics of transmitted and reflected photons in strong coupling regime. The parameters are the same as in Fig. 2(c) except $\Omega_p = 1$.

if $g^{(2)}(0) > 1$, then the field has a super-Poissonian statistics (e.g., for the single-mode thermal field $g^{(2)}(0) = 2$) [9]. Correlation functions are plotted on Figs. 5 and 6, respectively, for the strong-coupling and bad cavity limits, varying on the x axis the control field and on the y axis the physical parameter of interest. Here we truncate $g^{(2)}(0)$ function for values higher than 2 for convenience of graphical representation, since the regions of quantum light [$g^{(2)}(0) < 1$] are easily noticeable in this case. We remark, that this kind of truncation still keeps all information about the statistics of the light only omitting the regions of extreme bunching which is not of interest in the current manuscript.

As we can see from the second column of Fig. 5, in the regime of functional switch (here $g > \kappa_{\rm ex}$) reflected light remains in the coherent state. To understand why this is the case, we write an expression for the reflected output field and take into account the $\langle A\rangle \approx 0$, as was demonstrated in Fig. 2. Then

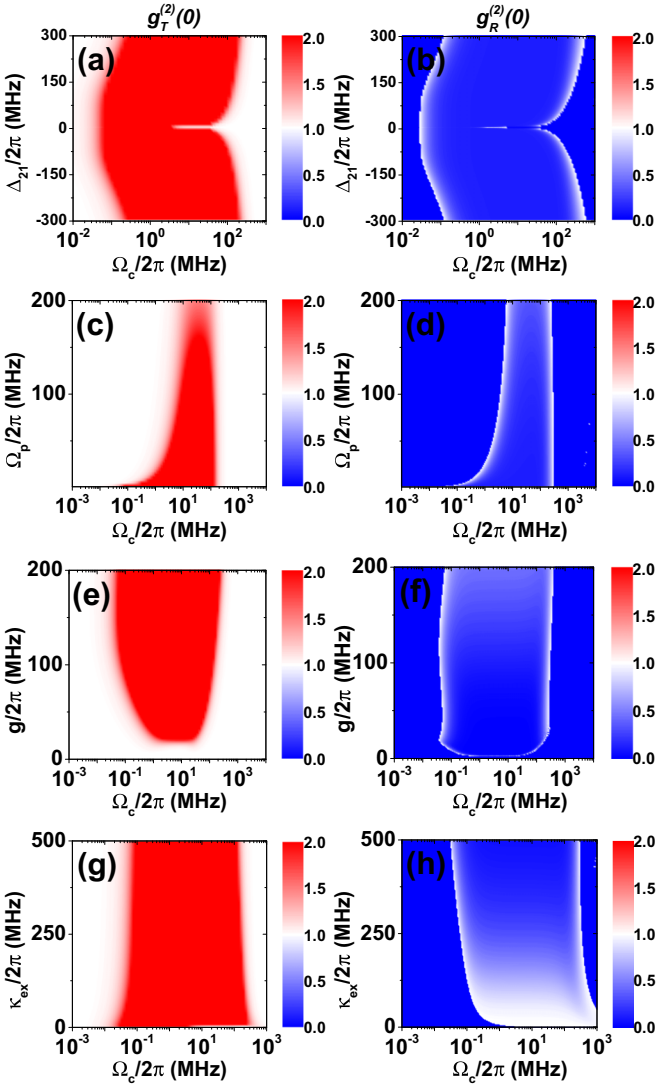

FIG. 6. Contour plots for the photon statistics of transmitted and reflected photons in bad-cavity regime. The parameters are the same as in Fig. 2(g) except $\Omega_p = 1$.

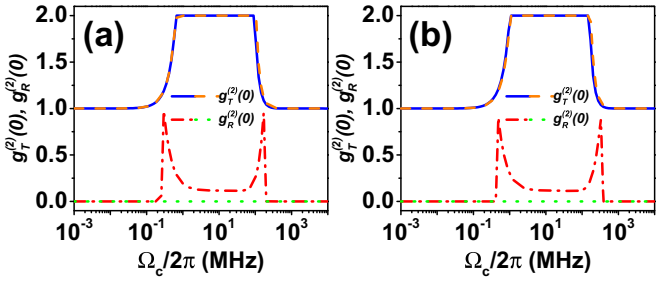

FIG. 7. Panels (a) and (b) are the comparison between numerical simulation and adiabatic elimination for Figs. 2(e) and 2(g).

we can estimate, that $b_{\text{out,ex}} \approx \sqrt{\kappa}B$, here we took into account that $\langle b_{\text{in,ex}}\rangle = 0$. The normal mode $\langle\sqrt{\kappa}B\rangle = -i\Omega_p\sqrt{2\kappa} = \langle a_{\text{in}}\rangle$, which means mode B has the same statistics as the input field (this has been numerically demonstrated in Ref. [25]), which is assumed to be in the coherent state.

In contrast, in bad cavity limit the reflected light becomes quantum as $g_R^2(0) \ll 1$, which corresponds to the dark/blue regions of the Fig. 6. This is a result of a nonconventional photon blockade [22] and can be understood by studying the output reflected field. After making an adiabatic elimination of cavity modes, which we outline in great detail in the Appendix, for calculating average values we use the following mapping: $b_{\text{out,ex}} \to \beta_0 + \beta_- \sigma_{1e}$. Moreover, in the case when $\Delta_r = 0$ and $h = 0$, the parameter $\beta_0 = 0$, which means reflected photons are solely generated by an atom. After an atom emits the photon it is projected into its ground state, and it takes finite amount of time, given by $1/\Gamma$, where Γ is the Purcell enhanced decay rate [50] (see the Appendix for the expression of Γ), for it to get re-excited and emit a photon again. This also can be showed, from the analytical Eq. (A10), from which it immediately follows that $g_R^2(0) = 0$, which corresponds to the single photon statistics [as its been mentioned for the Fock state $|n\rangle$, $g^{(2)}(0) = 1 - 1/n$, so when $n = 1$, $g^{(2)}(0) = 0$]. It is important to notice that $g_R^2(0) = 0$ does not hold in our numerical simulations, and $g_R^2(0) \approx 0.1$, since we are considering the case $\kappa = 2g$, and not really in the bad cavity limit, where $\kappa \gg g$.

For the transmitted field interesting features appear because of the interference between the straight-through transmission of the coherent driving field and the forward scattered fluorescence from the atom. The consequences of this interference on the photon statistics were first time noted in the Ref. [51], for the single-atom interacting with a single mode-cavity in a bad-cavity limit. As we can see from the first columns of Figs. 5 and 6, in the regions of switch functionality, transmitted light shows bunching behavior (dark/red regions) as a result of destructive interference between the field radiated by the atom and an intracavity field. This behavior in terms of normal modes A and B, has been explained in great detail in Ref. [44], and it turns out that bunching behavior is a consequence of normal mode A being strongly bunched (we have numerically verified that this holds for our system in both limits).

As it can be seen in Fig. 7 analytical and numerical results for the two-photon correlation function agree well, in the bad-cavity limit (as it was previously mentioned in the strong coupling analytical approach fails to predict correct correlation function, which is expected), with a drawback that numerical approach starts failing for obtaining $g_R^{(2)}(0)$ out of the switch functionality region, where we simply set it to zero, when it obtains values bigger than one. This happens because of the divergence of normalized two-photon correlation function, when photon flux is zero and no photons are detected (this gets even more apparent by considering correlation function for the Fock state $|n\rangle$, $g2(0) = 1 - 1/n$ which diverges when $n = 0$). This remark is substantiated by the fact that for the finite value of h, analytical and numerical approaches start to agree better with increasing value of h, because the photon flux for the reflected field never gets equal to zero. To summarize, $g_R^{(2)}(0) = 0$ for the all values of Ω_c; however, photodetection is going to reveal antibunched statistics in the region of switch functionality, and no photons will be detected out of this region.

V. GENERATION OF THE ATOM-LIGHT ENTANGLED STATE

In this section we briefly outline the protocol for generating the entangled state between the transmitted and reflected coherent light states and the atom. The possibility of generating such a state shows that the switch is indeed quantum, as entanglement is an inherent property of the quantum systems. To achieve this task we need an additional auxiliary metastable ground level $|3\rangle$, and thus now we have the tripod atomic configuration. Tripod systems have been used in quantum optics for generating the time-bin qubits, which exhibit an entanglement between two temporal modes [52] as well for creating large nonlinear Kerr coupling between the two fields which was utilized to generate the entanglement between them [53].

To generate the entangled state it is enough to prepare the atom in the initial state $|\Psi_{\text{in}}\rangle = \frac{1}{\sqrt{2}}(|2\rangle + |3\rangle)$, which can be achieved with microwave or radio-frequency field coupling the respective states and creating their coherent superposition. The protocol works as follows: if the atom is in the state $|3\rangle$, then light simply passes through the system and an incoming coherent state $|\alpha\rangle$ is the output field from the channel $a_{\text{out,ex}}$ and the combined system ends up in the state $|3\rangle \otimes |\alpha\rangle$; however, if the atom is initially in the state $|2\rangle$, then under the conditions of system working as switch the light pulse is reflected and transferred into the channel $b_{\text{out,ex}}$ and the final state of the system is $|2\rangle \otimes |-\alpha\rangle$. In other words, the following transformation can be achieved in our system for creating light-atom entangled state:

$$|\Psi_{\text{in}}\rangle \otimes |0\rangle_{b_{\text{in,ex}}}|\alpha\rangle_{a_{\text{in,ex}}} \rightarrow \frac{1}{\sqrt{2}} \times [|3\rangle \otimes |\alpha\rangle_{a_{\text{out,ex}}}|0\rangle_{b_{\text{out,ex}}} + |2\rangle \otimes |-\alpha\rangle_{b_{\text{out,ex}}}|0\rangle_{a_{\text{out,ex}}}]. \tag{14}$$

We comment that achieving this entangled state is not a trivial task as there are decoherence channels in the system (atom and cavity decay rates) and we plan to address the calculation of the fidelity of entangled state preparation in the future publication. It is interesting to point out that with suitable unitary rotations and projective measurements state Eq. (14) can be transferred into the conventional cat state. This state is of significant interest in the context of quantum computing and metrology [5]. Once the Cat state is achieved it means that switch is projected into the superposition of the "on" and "off" states which is one more signature of switch being quantum switch.

VI. CONCLUSIONS

In this paper, we suggest new scheme for realizing quantum switch for an incoming coherent field. Our scheme is based on the coupling the fiber-coupled ring cavity with a single Λ-level atom. We have demonstrated both numerically and analytically that it is possible to tune the system by the external control field from being fully transparent to being fully reflective. We emphasize that our proposal has an advantage of being easily implemented experimentally, compared to other proposals which require high control over the "gate valve" parameter, which is not easily achievable in current experiments. Here, we have concluded that the switch functions both in strong coupling and weak coupling limits, under the condition of strong fiber-over-coupling (showing better performance in the strong-coupling limit) for the reasonably large amplitude of the incoming field (up to $\approx$50MHz, when $g > \kappa_{\text{ex}}$, up to $\approx$40MHz, when $g < \kappa_{\text{ex}}$). Moreover, we have demonstrated that the regime of functionality can be extended by increasing two-photon detuning and found the optimal value for it in the strong coupling regime. Moreover, we have obtained analytical results in the bad-cavity limit through adiabatic elimination of cavity modes, and they are in good agreement with numerical simulations of respective master equations. Surprisingly, this approach works even in the strong coupling limit showing qualitative agreement for transmitted and reflected field intensities. It is important to mention that our protocol works only for nonzero two-photon detuning which means that we are not using conventional EIT-based approach.

By studying the statistics of transmitted and reflected fields, we have verified that quantum switch does not modify the state of the incoming coherent field in the strong coupling limit; however, in the bad-cavity limit our system can produce quantum states of light in the reflected field. So in bad-cavity limit our system can be used as a "black box" which acts as a quantum device which takes as input coherent field and gives quantum light in the output.

We also briefly discussed a possibility of the atom-light entangled state generation. We emphasize that the possibility of our switch being in entangled state as well being in the superpositions of the "on" and "off" states shows that it is indeed a quantum switch.

Our proposal has a potential interest in realizing quantum information protocols with coherent light states. For future projects, it would be interesting to concatenate several ring cavities to fiber and study if the system can work as a photon router for a few-photon incoming state. It also would be of interest to implement quantum repeater schemes such as DLCZ [54,55].

In addition, there have been several interesting theoretical proposals on coupling NV centers with ring cavities for generating entangled states between the color centers [56–59]. Since color centers are solid-state systems there is no need to trap them as it is the case with cold atoms. Moreover, in the recent experimental realization a single photon source based on coupling ring cavity with SiV vacancies has been realized [60]. So it would be interesting to implement a quantum switch by coupling ring resonators with color centers, which have a multilevel structure and can be utilized as Λ-level systems.

ACKNOWLEDGMENTS

D.A., L.C.K., and L.K. acknowledge support from NRF Grant No. 2014NRF-CRP002-042. The IHPC A*STAR Team acknowledges the National Research Foundation Singapore (Grants No. NRF2017NRF-NSFC002-015, No. NRF2016-NRF-ANR002, and No. NRF-CRP 14-2014-04) and A*STAR SERC (Grant No. A1685b0005). D.A. acknowledges A. Chia for stimulating discussions. D.A. thanks Prof. P. Sharapova for supporting this work on its early stages. D.A. also

acknowledges Stella Seah for insightful discussions on Markovian master equations.

APPENDIX: ADIABATIC ELIMINATION

In the bad cavity limit ($\kappa \gg \gamma, g$), we can adiabatically eliminate the lossy cavity mode and obtain an effective model for the three-level atom [10,22]. By expressing cavity modes through the normal modes A and B, the Hamiltonian Eq. (1) can be recast into Eq. (7), where $g_A = \sqrt{2}\mathrm{Re}[g]$ and $g_B = \sqrt{2}\mathrm{Im}[g]$. After writing the Heisenberg equations for the normal modes in the framework of the input-output theory [48], we obtain the following expressions:

$$\begin{aligned}\dot{A} =& -i\left[(\Delta_r + h - i\kappa/2)A + g_A\sigma_{1e} + \frac{\Omega_p}{\sqrt{2}}\right] \\ & - \sqrt{\kappa_{\mathrm{ex}}}A_{\mathrm{in,ex}} - \sqrt{\kappa_{\mathrm{i}}}A_{\mathrm{in,i}}, \\ \dot{B} =& -i\left[(\Delta_r - h - i\kappa/2)B - ig_B\sigma_{1e} + \frac{\Omega_p}{\sqrt{2}}\right] \\ & - \sqrt{\kappa_{\mathrm{ex}}}B_{\mathrm{in,ex}} - \sqrt{\kappa_{\mathrm{i}}}B_{\mathrm{in,i}}. \end{aligned} \tag{A1}$$

It is easy to show that the steady-state amplitudes of empty cavity ($g = 0$) fields can be expressed as

$$\begin{aligned}\alpha_A = \langle A\rangle &= -\frac{\Omega_p}{\sqrt{2}}\frac{1}{\Delta_r + h - i\kappa/2}, \\ \alpha_B = \langle B\rangle &= -\frac{\Omega_p}{\sqrt{2}}\frac{1}{\Delta_r - h - i\kappa/2}. \end{aligned} \tag{A2}$$

We have used the following relations $\langle A_{\mathrm{in,ex}}\rangle = \langle B_{\mathrm{in,ex}}\rangle = -i * \Omega_p/\sqrt{k_{\mathrm{ex}}}$, which follows from our initial conditions for $a_{\mathrm{in,ex}}$ and $b_{\mathrm{in,ex}}$. Also we assume that cavity initially is in the vacuum state which means $\langle A_{\mathrm{in,i}}\rangle = \langle B_{\mathrm{in,i}}\rangle = 0$ are both zero. To adiabatically eliminate the cavity modes, we formally integrate the operators of A and B and substitute them into the optical Bloch equation for the atom. After integration and taking into account that we are in the bad cavity limit, inside the integrals of for the normal cavity modes, the atomic correlation functions may be evaluated at $t' = t$, thus we use the Markov approximation. After evaluating the integrals cavity normal modes takes the form

$$\begin{aligned}A(t) &= \alpha_A - \frac{ig_A\sigma_{1e}(t) + \sqrt{\kappa_{\mathrm{ex}}}A_{\mathrm{in,ex}}(t) + \sqrt{\kappa_{\mathrm{i}}}A_{\mathrm{in,i}}(t)}{i(\Delta_r + h - i\kappa/2)}, \\ B(t) &= \alpha_B - \frac{g_B\sigma_{1e}(t) + \sqrt{\kappa_{\mathrm{ex}}}B_{\mathrm{in,ex}}(t) + \sqrt{\kappa_{\mathrm{i}}}B_{\mathrm{in,i}}(t)}{i(\Delta_r - h - i\kappa/2)}. \end{aligned} \tag{A3}$$

The averages of σ_{1e} and σ_{12} are given by

$$\begin{aligned}\langle\dot{\sigma_{1e}}\rangle =& -i(\Delta_{e1} - i\Gamma/2)\langle\sigma_{1e}\rangle + ig_A\langle(\sigma_{ee} - \sigma_{11})A\rangle \\ & - g_B\langle(\sigma_{ee} - \sigma_{11})B\rangle - i\Omega_c\langle\sigma_{12}\rangle, \\ \langle\dot{\sigma_{12}}\rangle =& -i\Delta_{21}\langle\sigma_{12}\rangle + ig_A\langle\sigma_{e2}A\rangle - g_B\langle\sigma_{e2}B\rangle - i\Omega_c\langle\sigma_{1e}\rangle. \end{aligned} \tag{A4}$$

In the bad-cavity limit the cavity field correlation time is very short compared to the atomic decay timescale. Thus, we have, for example,

$$\langle\sigma_{ee}(t)A(0)\rangle = \langle\sigma_{ee}(t)A_{\mathrm{in,ex}}(t')\rangle = \langle\sigma_{ee}(t)A_{\mathrm{in,i}}(t')\rangle = 0. \tag{A5}$$

After substituting Eqs. (A3) into the Eqs. (A4), we obtain

$$\begin{aligned}\langle\dot{\sigma_{1e}}\rangle &= -i(\Delta'_{e1} - i\Gamma'/2)\langle\sigma_{1e}\rangle + i\Omega'_p\langle\sigma_{ee} - \sigma_{11}\rangle - i\Omega_c\langle\sigma_{12}\rangle, \\ \langle\dot{\sigma_{12}}\rangle &= -i\Delta_{21}\langle\sigma_{12}\rangle + i\Omega'_p\langle\sigma_{e2}\rangle - i\Omega_c\langle\sigma_{1e}\rangle, \end{aligned} \tag{A6}$$

where

$$\begin{aligned}\Delta'_{e1} &= \Delta_{e1} - \frac{g_A^2(\Delta_r + h)}{(\Delta_r + h)^2 + (\kappa/2)^2} - \frac{g_B^2(\Delta_r - h)}{(\Delta_r - h)^2 + (\kappa/2)^2}, \\ \Gamma'_{e1} &= \Gamma_{e1} + \frac{g_A^2\kappa}{(\Delta_r + h)^2 + (\kappa/2)^2} + \frac{g_B^2\kappa}{(\Delta_r - h)^2 + (\kappa/2)^2}, \\ \Omega'_p &= g_A\alpha_A + ig_B\alpha_B, \Gamma' = \Gamma'_{e1} + \Gamma_{e2}. \end{aligned} \tag{A7}$$

Therefore, the cavity modes are adiabatically eliminated. Notice that $\langle\dot{\sigma_{22}}\rangle = -i\Omega_c(\langle\sigma_{2e}\rangle - \langle\sigma_{e2}\rangle) + \Gamma_{e2}\langle\sigma_{ee}\rangle$, the effective master equation for the three-level atom is

$$\dot{\rho}_{\mathrm{a}} = -i[H_{\mathrm{a}}, \rho_{\mathrm{a}}] + \frac{\Gamma'_{e1}}{2}\mathcal{D}[\sigma_{1e}]\rho_{\mathrm{a}} + \frac{\Gamma_{e2}}{2}\mathcal{D}[\sigma_{2e}]\rho_{\mathrm{a}}, \tag{A8}$$

where $H_{\mathrm{a}} = \Delta'_{e1}\sigma_{ee} + \Delta_{21}\sigma_{22} + \Omega'_p\sigma_{e1} + \Omega'^*_p\sigma_{1e} + \Omega_c(\sigma_{2e} + \sigma_{e2})$. To summarize, we mapped the entire system of the atom coupled to the fiber-coupled microtoroidal cavity to the effective system which is represented by a three-level atom, which has Purcell enhanced decay rate and detuning on the $e - 1$ leg of Λ system, and is coupled to the classical fields Ω'_p and Ω_c, respectively, on the transitions $e - 1$ and $2 - e$. We remark that correlation functions for the output fields can be calculated by making the following

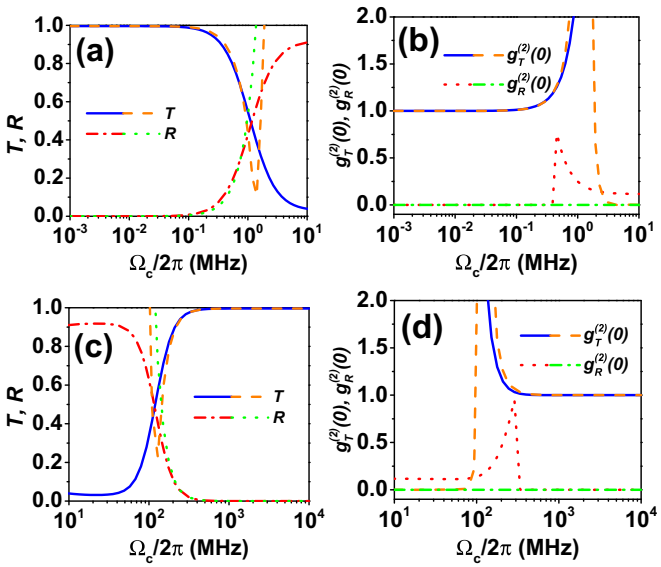

FIG. 8. Taylor expansion for Fig. 2(g). Panels (a) and (b) are the Taylor expansion of transmission, reflection, and correlations when $\Omega_c \to 0$; panels (c) and (d) are the Taylor expansion of transmission, reflection, and correlations when $\Omega_c \to \infty$.

substitutions:

$$
\begin{aligned}
&a_{\mathrm{out,ex}} \to \alpha_0 + \alpha_- \sigma_{1e},\\
&b_{\mathrm{out,ex}} \to \beta_0 + \beta_- \sigma_{1e},\\
&\alpha_0 = \frac{i\Omega_p}{\sqrt{\kappa_{\mathrm{ex}}}} + \sqrt{\kappa_{\mathrm{ex}}/2}(\alpha_A + \alpha_B),\\
&\alpha_- = -\sqrt{\kappa_{\mathrm{ex}}/2}\left[\frac{ig_A}{i(\Delta_r + h - i\kappa/2)} + \frac{g_B}{i(\Delta_r - h - i\kappa/2)}\right],\\
&\beta_0 = \sqrt{\kappa_{\mathrm{ex}}/2}(\alpha_A - \alpha_B),\\
&\beta_- = -\sqrt{\kappa_{\mathrm{ex}}/2}\left[\frac{ig_A}{i(\Delta_r + h - i\kappa/2)} - \frac{g_B}{i(\Delta_r - h - i\kappa/2)}\right];
\end{aligned}
\tag{A9}
$$

after substituting these expressions into the numerators of the Eqs. (5) and (13) we obtain

$$
\begin{aligned}
\langle a^\dagger_{\mathrm{out,ex}} a_{\mathrm{out,ex}}\rangle_{\mathrm{ss}} &= |\alpha_0|^2 + \alpha_0^*\alpha_-\rho^{\mathrm{ss}}_{e1} + \alpha_0\alpha_-^*\rho^{\mathrm{ss}}_{1e} + |\alpha_-|^2\rho^{\mathrm{ss}}_{ee},\ \langle b^\dagger_{\mathrm{out,ex}} b_{\mathrm{out,ex}}\rangle_{\mathrm{ss}}\\
&= |\beta_0|^2 + \beta_0^*\beta_-\rho^{\mathrm{ss}}_{e1} + \beta_0\beta_-^*\rho^{\mathrm{ss}}_{1e} + |\beta_-|^2\rho^{\mathrm{ss}}_{ee},\ \langle a^\dagger_{\mathrm{out,ex}} a^\dagger_{\mathrm{out,ex}} a_{\mathrm{out,ex}} a_{\mathrm{out,ex}}\rangle_{\mathrm{ss}}\\
&= |\alpha_0|^2\big(|\alpha_0|^2 + 2\alpha_0^*\alpha_-\rho^{\mathrm{ss}}_{e1} + 2\alpha_0\alpha_-^*\rho^{\mathrm{ss}}_{1e} + 4|\alpha_-|^2\rho^{\mathrm{ss}}_{ee}\big),\ \langle b^\dagger_{\mathrm{out,ex}} b^\dagger_{\mathrm{out,ex}} b_{\mathrm{out,ex}} b_{\mathrm{out,ex}}\rangle_{\mathrm{ss}}\\
&= |\beta_0|^2\big(|\beta_0|^2 + 2\beta_0^*\beta_-\rho^{\mathrm{ss}}_{e1} + 2\beta_0\beta_-^*\rho^{\mathrm{ss}}_{1e} + 4|\beta_-|^2\rho^{\mathrm{ss}}_{ee}\big),
\end{aligned}
\tag{A10}
$$

where $\rho^{\mathrm{ss}}_{e1} = \langle\sigma_{1e}\rangle_{\mathrm{ss}}$, $\rho^{\mathrm{ss}}_{1e} = \langle\sigma_{e1}\rangle_{\mathrm{ss}}$, $\rho^{\mathrm{ss}}_{ee} = \langle\sigma_{ee}\rangle_{\mathrm{ss}}$. By solving Eq. (A8) for the effective three-level system, the elements of the steady-state density matrix are given by

$$
\rho^{\mathrm{ss}}_{ee} = \frac{a_2\Omega_c^2}{c_0 + c_2\Omega_c^2 + c_4\Omega_c^4 + c_6\Omega_c^6}, \quad \rho^{\mathrm{ss}}_{1e} = \frac{b_2\Omega_c^2 + b_4\Omega_c^4}{c_0 + c_2\Omega_c^2 + c_4\Omega_c^4 + c_6\Omega_c^6},
\tag{A11}
$$

where $a_2 = |\Omega_p'|^2\Delta_{21}^2\Gamma$, $b_2 = \Omega_p'^*\Delta_{21}[\Gamma_{e2}|\Omega_p'|^2 - \Delta_{21}\Gamma'_{e1}(\Delta'_{e1} - i\Gamma/2)]$, $b_4 = \Omega_p'^*\Delta_{21}\Gamma'_{e1}$, $c_0 = \Gamma_{e2}|\Omega_p'|^2||\Omega_p'|^2 - \Delta_{21}^2 + \Delta_{21}(\Delta'_{e1} - i\Gamma/2)|^2$, $c_2 = \Gamma'_{e1}\Delta_{21}^2|\Delta'_{e1} - i\Gamma/2|^2 + 2\Gamma\Delta_{21}^2|\Omega_p'|^2 + (\Gamma + \Gamma_{e2})|\Omega_p'|^4$, $c_4 = -2\Gamma'_{e1}\Delta_{21}\Delta'_{e1} + (\Gamma + \Gamma_{e2})|\Omega_p'|^2$, $c_6 = \Gamma'_{e1}$, and $\Gamma = \Gamma'_{e1} + \Gamma_{e2}$. We remark that when $\Delta_{21} = 0$, $\rho_{1e} = 0$ as it follows from Eq. (A11) and is a consequence of coherent population trapping. This clearly shows that for obtaining a quantum transistor we need a nonzero two photon detuning. To simplify the lengthy expressions for the intensities and correlation functions in certain limits, we resume to Taylor expanding the density matrix elements in the limits of small and large driving fields, we find that when $\Omega_c \to 0$, $\rho^{\mathrm{ss}}_{ee} \approx \frac{a_2}{c_0}\Omega_c^2$ and $\rho^{\mathrm{ss}}_{1e} \approx \frac{b_2}{c_0}\Omega_c^2$; however, when $\Omega_c \to \infty$, $\rho^{\mathrm{ss}}_{ee} \approx \frac{a_2}{c_6}\Omega_c^{-4} - \frac{a_2c_4}{c_6^2}\Omega_c^{-6}$ and $\rho^{\mathrm{ss}}_{1e} \approx \frac{b_4}{c_6}\Omega_c^{-2} + \frac{b_2c_6 - b_4c_4}{c_6^2}\Omega_c^{-4}$. It is straightforward to demonstrate by using these expressions that in both limits $\rho_{1e} \approx 0$, which means that atoms is decoupling from the cavity in this limit (note that absorption is given by the imaginary part of the off-diagonal term of the density matrix).

After substituting these expressions into Eqs. (A10), we have in the limit $\Omega_c \to 0$,

$$
\begin{aligned}
T &= \frac{|\alpha_0|^2 + (2\mathrm{Re}[\alpha_0\alpha_-^* b_2/c_0] + |\alpha_-|^2 a_2/c_0)\Omega_c^2}{|\Omega_p|^2/2\kappa_{ex}},\\
R &= \frac{|\beta_0|^2 + (2\mathrm{Re}[\beta_0\beta_-^* b_2/c_0] + |\beta_-|^2 a_2/c_0)\Omega_c^2}{|\Omega_p|^2/2\kappa_{ex}},\\
g^{(2)}_{\mathrm{T}}(0) &= \frac{|\alpha_0|^2\big\{|\alpha_0|^2 + 4(\mathrm{Re}[\alpha_0\alpha_-^* b_2/c_0] + |\alpha_-|^2 a_2/c_0)\Omega_c^2\big\}}{\{|\alpha_0|^2 + (2\mathrm{Re}[\alpha_0\alpha_-^* b_2/c_0] + |\alpha_-|^2 a_2/c_0)\Omega_c^2\}^2},\\
g^{(2)}_{\mathrm{R}}(0) &= \frac{|\beta_0|^2\big\{|\beta_0|^2 + 4(\mathrm{Re}[\beta_0\beta_-^* b_2/c_0] + |\beta_-|^2 a_2/c_0)\Omega_c^2\big\}}{\{|\beta_0|^2 + (2\mathrm{Re}[\beta_0\beta_-^* b_2/c_0] + |\beta_-|^2 a_2/c_0)\Omega_c^2\}^2};
\end{aligned}
\tag{A12}
$$

and for the limit $\Omega_c \to \infty$ we obtain

$$
\begin{aligned}
T &= \frac{|\alpha_0|^2 + 2\mathrm{Re}[\alpha_0\alpha_-^* b_4/c_6]\Omega_c^{-2} + \big\{2\mathrm{Re}\big[\alpha_0\alpha_-^*(b_2c_6 - b_4c_4)/c_6^2\big] + |\alpha_-|^2 a_2/c_6\big\}\Omega_c^{-4} - |\alpha_-|^2 a_2c_4/c_6^2\Omega_c^{-6}}{|\Omega_p|^2/2\kappa_{ex}},\\
R &= \frac{|\beta_0|^2 + 2\mathrm{Re}[\beta_0\beta_-^* b_4/c_6]\Omega_c^{-2} + \big\{2\mathrm{Re}\big[\beta_0\beta_-^*(b_2c_6 - b_4c_4)/c_6^2\big] + |\beta_-|^2 a_2/c_6\big\}\Omega_c^{-4} - |\beta_-|^2 a_2c_4/c_6^2\Omega_c^{-6}}{|\Omega_p|^2/2\kappa_{ex}},
\end{aligned}
$$

$$g_{\mathrm{T}}^{(2)}(0)=\frac{|\alpha_0|^2\left(|\alpha_0|^2+4\mathrm{Re}[\alpha_0\alpha_-^*b_4/c_6]\Omega_c^{-2}+4\left\{\mathrm{Re}\left[\alpha_0\alpha_-^*(b_2c_6-b_4c_4)/c_6^2\right]+|\alpha_-|^2a_2/c_6\right\}\Omega_c^{-4}-4|\alpha_-|^2a_2c_4/c_6^2\Omega_c^{-6}\right)}{\left(|\alpha_0|^2+2\mathrm{Re}[\alpha_0\alpha_-^*b_4/c_6]\Omega_c^{-2}+\left\{2\mathrm{Re}\left[\alpha_0\alpha_-^*(b_2c_6-b_4c_4)/c_6^2\right]+|\alpha_-|^2a_2/c_6\right\}\Omega_c^{-4}-|\alpha_-|^2a_2c_4/c_6^2\Omega_c^{-6}\right)^2},$$

$$g_{\mathrm{R}}^{(2)}(0)=\frac{|\beta_0|^2\left(|\beta_0|^2+4\mathrm{Re}[\beta_0\beta_-^*b_4/c_6]\Omega_c^{-2}+4\left\{\mathrm{Re}\left[\beta_0\beta_-^*(b_2c_6-b_4c_4)/c_6^2\right]+|\beta_-|^2a_2/c_6\right\}\Omega_c^{-4}-4|\beta_-|^2a_2c_4/c_6^2\Omega_c^{-6}\right)}{\left(|\beta_0|^2+2\mathrm{Re}[\beta_0\beta_-^*b_4/c_6]\Omega_c^{-2}+\left\{2\mathrm{Re}\left[\beta_0\beta_-^*(b_2c_6-b_4c_4)/c_6^2\right]+|\beta_-|^2a_2/c_6\right\}\Omega_c^{-4}-|\beta_-|^2a_2c_4/c_6^2\Omega_c^{-6}\right)^2}. \tag{A13}$$

To demonstrate these results we compare Taylor expansion results with analytical results for the adiabatic elimination in Fig. 8.

[1] H. J. Kimble, Nature **453**, 1023 (2008).

[2] M. A. Nielsen and I. L. Chuang, *Quantum Computation and Quantum Information* (Cambridge University Press, Cambridge, 2000).

[3] P. Zoller, T. Beth, D. Binosi, R. Blatt, H. Briegel, D. Bruss, T. Calarco, J. I. Cirac, D. Deutsch, J. Eisert, A. Ekert, C. Fabre, N. Gisin, P. Grangiere, M. Grassl, S. Haroche, A. Imamoglu, A. Karlson, J. Kempe, L. Kouwenhoven, S. Kröll, G. Leuchs, M. Lewenstein, D. Loss, N. Lütkenhaus, S. Massar, J. E. Mooij, M. B. Plenio, E. Polzik, S. Popescu, G. Rempe, A. Sergienko, D. Suter, J. Twamley, G. Wendin, R. Werner, A. Winter, J. Wrachtrup, and A. Zeilinger, Eur. Phys. J. D: Atom. Mol. Optic. Plasma Phys. **36**, 203 (2005).

[4] N. Gisin and R. Thew, Nat. Photon. **1**, 165 (2007).

[5] V. Giovannetti, S. Lloyd, and L. Maccone, Science **306**, 1330 (2004).

[6] V. Giovannetti, S. Lloyd, and L. Maccone, Nat. Photon. **5**, 222 (2011).

[7] S. Haroche and D. Kleppner, Phys. Today **42**(1), 24 (1989).

[8] H. Walther, B. T. H. Varcoe, B.-G. Englert, and T. Becker, Rep. Progr. Phys. **69**, 1325 (2006).

[9] M. O. Scully and M. S. Zubairy, *Quantum Optics* (Cambridge University Press, Cambridge, 1997).

[10] H. Charmichael, *Statistical Methods in Quabtum Optics II* (Springer-Verlag, Berlin/Heidelberg, 2008).

[11] J. M. Raimond, M. Brune, and S. Haroche, Rev. Mod. Phys. **73**, 565 (2001).

[12] S. Ritter, C. Nölleke, C. Hahn, A. Reiserer, A. Neuzner, M. Uphoff, M. Mücke, E. Figueroa, J. Bochmann, and G. Rempe, Nature **484**, 195 (2012).

[13] J. I. Cirac, P. Zoller, H. J. Kimble, and H. Mabuchi, Phys. Rev. Lett. **78**, 3221 (1997).

[14] A. Reiserer and G. Rempe, Rev. Mod. Phys. **87**, 1379 (2015).

[15] K. J. Vahala, Nature **424**, 839 (2003).

[16] T. Aoki, B. Dayan, E. Wilcut, W. P. Bowen, A. S. Parkins, T. J. Kippenberg, K. J. Vahala, and H. J. Kimble, Nature **443**, 671 (2006).

[17] T. Aoki, A. S. Parkins, D. J. Alton, C. A. Regal, B. Dayan, E. Ostby, K. J. Vahala, and H. J. Kimble, Phys. Rev. Lett. **102**, 083601 (2009).

[18] K. Srinivasan and O. Painter, Nature **450**, 862 (2007).

[19] D. O'Shea, C. Junge, J. Volz, and A. Rauschenbeutel, Phys. Rev. Lett. **111**, 193601 (2013).

[20] T. J. Kippenberg, S. M. Spillane, and K. J. Vahala, Appl. Phys. Lett. **85**, 6113 (2004).

[21] I. Shomroni, S. Rosenblum, Y. Lovsky, O. Bechler, G. Guendelman, and B. Dayan, Science **345**, 903 (2014).

[22] B. Dayan, A. S. Parkins, T. Aoki, E. P. Ostby, K. J. Vahala, and H. J. Kimble, Science **319**, 1062 (2008).

[23] V. V. Klimov, M. Ducloy, and V. S. Letokhov, Phys. Rev. A **59**, 2996 (1999).

[24] S. M. Spillane, T. J. Kippenberg, K. J. Vahala, K. W. Goh, E. Wilcut, and H. J. Kimble, Phys. Rev. A **71**, 013817 (2005).

[25] K. Srinivasan and O. Painter, Phys. Rev. A **75**, 023814 (2007).

[26] K. Srinivasan, M. Borselli, O. Painter, A. Stintz, and S. Krishna, Opt. Express **14**, 1094 (2006).

[27] J. L. O'Brien, A. Furusawa, and J. Vučković, Nature Photon. **3**, 687 (2009).

[28] T. Volz, A. Reinhard, M. Winger, A. Badolato, K. J. Hennessy, E. L. Hu, and A. Imamoğlu, Nature Photon. **6**, 605 (2012).

[29] M. Bajcsy, S. Hofferberth, V. Balic, T. Peyronel, M. Hafezi, A. S. Zibrov, V. Vuletic, and M. D. Lukin, Phys. Rev. Lett. **102**, 203902 (2009).

[30] X. Yang, M. Yu, D.-L. Kwong, and C. W. Wong, Phys. Rev. Lett. **102**, 173902 (2009).

[31] W. Chen, K. M. Beck, R. Bücker, M. Gullans, M. D. Lukin, H. Tanji-Suzuki, and V. Vuletić, Science **341**, 768 (2013).

[32] D. E. Chang, A. S. Sørensen, E. A. Demler, and M. D. Lukin, Nat. Phys. **3**, 807 (2007).

[33] H. Gorniaczyk, C. Tresp, J. Schmidt, H. Fedder, and S. Hofferberth, Phys. Rev. Lett. **113**, 053601 (2014).

[34] D. Tiarks, S. Baur, K. Schneider, S. Dürr, and G. Rempe, Phys. Rev. Lett. **113**, 053602 (2014).

[35] A. M. C. Dawes, L. Illing, S. M. Clark, and D. J. Gauthier, Science **308**, 672 (2005).

[36] D. A. Steck, *Quantum and Atom Optics* (2007), http://atomoptics-nas.uoregon.edu/~dsteck/teaching/quantum-optics/quantum-optics-notes.pdf.

[37] J. Volz and A. Rauschenbeutel, Science **341**, 725 (2013).

[38] M. T. Manzoni, F. Reiter, J. M. Taylor, and A. S. Sørensen, Phys. Rev. B **89**, 180502(R) (2014).

[39] L. Neumeier, M. Leib, and M. J. Hartmann, Phys. Rev. Lett. **111**, 063601 (2013).

[40] O. Kyriienko and A. S. Sørensen, Phys. Rev. Lett. **117**, 140503 (2016).

[41] F.-Y. Hong and S.-J. Xiong, Phys. Rev. A **78**, 013812 (2008).

[42] L.-M. Duan, J. I. Cirac, P. Zoller, and E. S. Polzik, Phys. Rev. Lett. **85**, 5643 (2000).

[43] B. Julsgaard, A. Kozhekin, and E. S. Polzik, Nature **413**, 400 (2001).

[44] S. Parkins and T. Aoki, Phys. Rev. A **90**, 053822 (2014).

[45] V. V. Klimov, V. S. Letokhov, and M. Ducloy, Laser Physics **17**, 912 (2007).

[46] J. Li, R. Yu, M. Liu, C. Ding, and X. Yang, Opt. Commun. **285**, 680 (2012).
[47] R. Yu, J. Li, M. Liu, C. Ding, and X. Yang, Opt. Commun. **284**, 5263 (2011).
[48] D. F. Walls and G. J. Milburn, *Quantum and Atom Optics* (Springer-Verlag, Berlin/Heidelberg, 1994).
[49] C. Navarrete-Benloch, arXiv:1504.05266v2 (2015).
[50] E. M. Purcell, Phys. Rev. **69**, 37 (1946).
[51] P. R. Rice and H. J. Carmichael, IEEE J. Quant. Electron. **24**, 1351 (1988).
[52] D. Aghamalyan and Y. Malakyan, in *Proceedings of the International Conference on Laser Physics 2010*, Vol. 7998 (International Society for Optics and Photonics, Bellingham, WA, 2011), p. 799815.
[53] D. Petrosyan and Y. P. Malakyan, Phys. Rev. A **70**, 023822 (2004).
[54] L.-M. Duan, M. D. Lukin, J. I. Cirac, and P. Zoller, Nature **414**, 413 (2001).
[55] D. Aghamalyan and Y. Malakyan, Phys. Rev. A **84**, 042305 (2011).
[56] F. Shi, X. Rong, N. Xu, Y. Wang, J. Wu, B. Chong, X. Peng, J. Kniepert, R.-S. Schoenfeld, W. Harneit, M. Feng, and J. Du, Phys. Rev. Lett. **105**, 040504 (2010).
[57] W. L. Yang, Z. Q. Yin, Z. Y. Xu, M. Feng, and J. F. Du, Appl. Phys. Lett. **96**, 241113 (2010).
[58] W. Yang, Z. Xu, M. Feng, and J. Du, New J. Phys. **12**, 113039 (2010).
[59] S. Liu, J. Li, R. Yu, and Y. Wu, Opt. Express **21**, 3501 (2013).
[60] J. Carolan, U. Chakraborty, N. C. Harris, M. Pant, T. Baehr-Jones, M. Hochberg, and D. Englund, Optica **6**, 335 (2019).